ELSEVIER

Journal of Power Sources 100 (2001) 149–163

JOURNAL OF POWER SOURCES

www.elsevier.com/locate/jpowsour

The sodium/nickel chloride (ZEBRA) battery

J.L. Sudworth

Beta Research and Development Ltd., 50 Goodsmoor Road, Sinfin, Derby DE24 9GN, UK

Abstract

This paper describes the operating principle, performance, production and applications of the sodium/nickel chloride (the so-called ZEBRA) battery.

Keywords: Battery; Sodium/nickel chloride; Temperature; Performance; Production; Applications

1. Introduction

The sodium/nickel chloride cell, like the sodium sulphur cell from which it evolved, consists of a liquid sodium negative electrode separated from a positive electrode by a sodium ion conducting solid electrolyte, beta alumina. It differs from the latter in that, a second, liquid, electrolyte (sodium chloroaluminate), is necessary to allow the rapid transport of sodium ions from the solid nickel chloride electrode to and from the ceramic electrolyte [1]. The melting point of this salt (157°C) determines the minimum operating temperature of the cell but optimum performance is obtained in the temperature range 270–350°C. At these temperatures, the beta alumina electrode contributes only a minor component to the cell resistance.

The normal cell reactions are as follows:

Positive electrode:

$$NiCl_2 + 2Na^+ + 2e^- \rightarrow Ni + 2NaCl \quad (1)$$

Negative electrode:

$$Na \rightarrow Na^+ + e^- \quad (2)$$

The net reaction is

$$NiCl_2 + 2Na \rightarrow 2NaCl + Ni, \quad E = 2.58\,V \quad (3)$$

Both anhydrous nickel chloride and sodium metal are very difficult to handle and it was discovered at a very early stage that it is possible to start with a completely discharged cell, i.e. nickel powder and sodium chloride, and to generate the sodium metal and nickel chloride by simply charging the cell [2]. The cell construction is shown schematically in Fig. 1 and the cell components are shown in Fig. 2. It can be seen that the metal foil wick which keeps the beta alumina tube covered with sodium metal during normal operation will also provide the electronic contact to the tube required to generate sodium metal on the first charge. Some of the sodium metal inevitably becomes trapped in the sodium compartment and is unavailable for electrochemical reaction. This would result in the cell capacity being limited by the negative electrode. This is undesirable as the end of discharge would be characterised by a sudden polarisation of the cell (Fig. 3). To avoid this, aluminium powder is incorporated in the positive electrode [3]. This allows the following reaction to occur:

$$Al + 4NaCl \rightarrow Na + NaAlCl_4, \quad E = 1.58\,V \quad (4)$$

The effect of this on the end-of-discharge characteristic can be seen in Fig. 4. The intermediate plateau which can be clearly seen are associated with the presence of sulphur in the electrode. This is added in the form of iron sulphide to stabilise the grain size of the nickel. Sulphur poisons the surface of the nickel crystals and prevents coherent layers of nickel being deposited from solution during discharge [4]. Although the solubility of nickel chloride is very low (7×10^{-4} mol/kg $NaAlCl_4$ at 250°C) [5], repeated electrical cycling leads to dissolution of nickel from the smaller nickel particles and deposition onto the larger particles. In the absence of sulphur, the average size of the nickel particles can increase from 1–2 μm to over 40 μm in 50 electrical cycles. This shows itself in the cell performance as a significant capacity loss. The addition of aluminium powder to the positive electrode has a secondary effect — as it dissolves to form sodium chloroaluminate, it leaves very fine pores distributed throughout the electrode. This porosity improves the high rate performance of the electrode.

E-mail address: jlsudworth@betard.co.uk (J.L. Sudworth).

0378-7753/01/$ – see front matter
PII: S0378-7753(01)00891-6

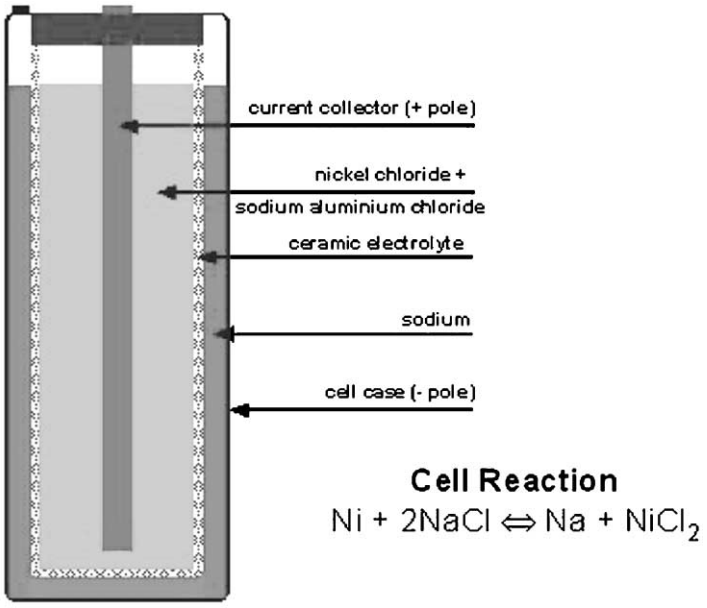

Fig. 1. Schematic diagram of ZEBRA cell.

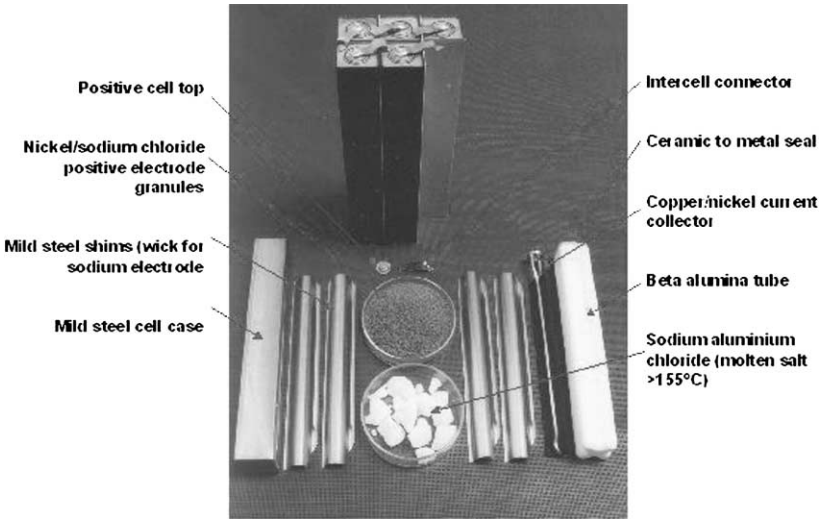

Fig. 2. ZEBRA components.

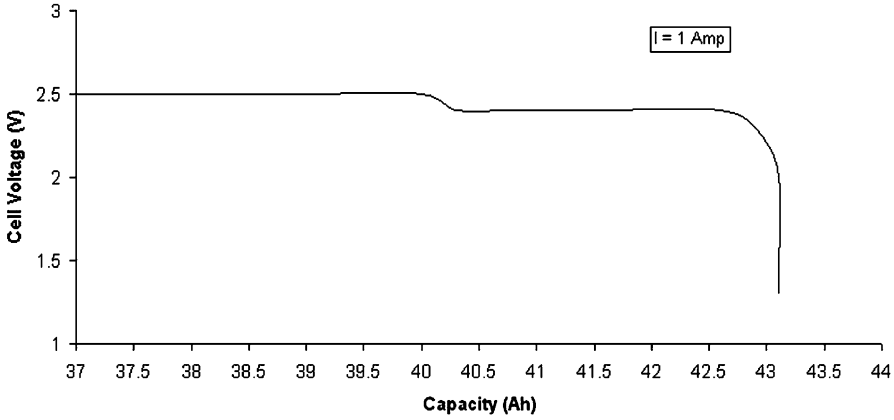

Fig. 3. Characteristics of first generation cell at end of discharge.

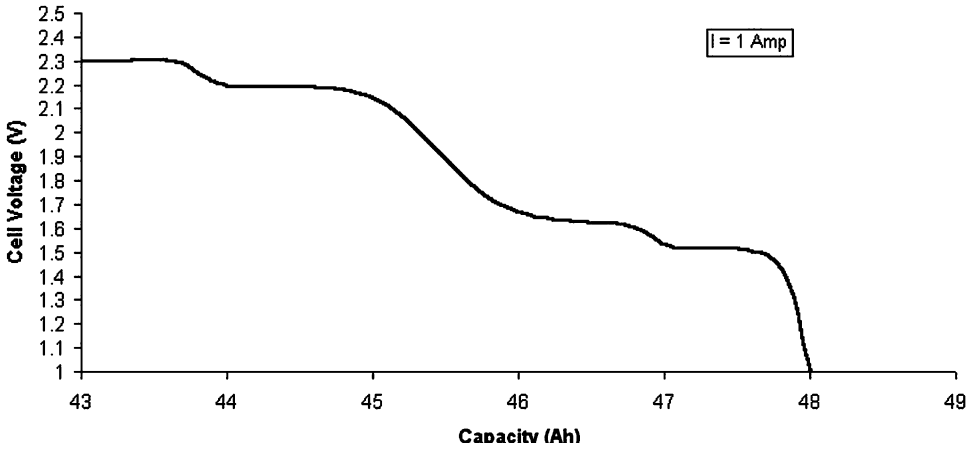

Fig. 4. Characteristics of second generation cell at end of discharge.

The voltage range of the sodium chloroaluminate electrolyte is ca. 1.5 V, and at the top of charge, it is decomposed in the following reaction:

$$2NaAlCl_4 + Ni \rightarrow NiCl_2 + 2Na + 2AlCl_3 \quad (5)$$

This reaction, rather than formation of chlorine gas, occurs because the amount of nickel in the positive electrode is approximately three times the stoichiometric quantity required for reaction (3).

This excess nickel provides the conducting backbone in the positive electrode and is necessary for stable cycling characteristics. Despite this excess nickel, the weight of nickel per kilowatthour is still one-third that of nickel metal hydride cells and half that of nickel cadmium cells.

The positive electrode material, which also contains small quantities of other sodium halides to stabilise the resistance over the life of the cell, is produced by blending the active materials: nickel, sodium chloride, iron sulphide and other sodium halides in the form of dry powders. To prevent segregation of the individual components and to provide an easily handled material, the blended powder is granulated using an industrial compactor. This granulate is poured into the positive electrode compartment whilst vibrating the cell. The weight of granulate is controlled to $\pm 0.5\%$ and this ensures that each cell has the same capacity. After a final drying operation to ensure that all traces of moisture are removed, the liquid sodium chloroaluminate is added and the positive electrode compartment is sealed by welding on a nickel cap. Although the nickel backbone provides sufficient radial conductivity in the electrode, a nickel current collector is required for longitudinal conduction to the cell terminal. This is fabricated as a double conductor so that a sheet of carbon felt can be held in place between the two parts (Fig. 2). This material is over 95% porous, so adds little to the cell weight. Its function is to keep the upper part of the porous electrode fully wetted by the sodium chloroaluminate.

On the first charge, sodium is generated at the points of contact between the metal shims and the beta alumina tube and quickly spreads out to cover the whole tube. This is aided by a coating of fine carbon powder which is applied to the tube in the form of an aqueous suspension before the cell is assembled. This provides a localised wicking action where the metal wick does not fit closely enough to the beta alumina tube. In the positive electrode, the second part of the first charge converts iron sulphide to ferrous chloride and nickel sulphide:

$$FeS + 2NaCl + Ni \rightarrow FeCl_2 + NiS + 2Na, \quad E = 2.37\,V \quad (6)$$

This is followed by the main cell reaction (3). The cell is fully charged when all the sodium chloride has been consumed. It is important to reach this point on the first cycle because of the way the electrode operates. The electronic conductivity of the nickel backbone is much greater than the ionic conductivity of the sodium chloroaluminate melt. This has the effect of biasing the electrode reaction to the region of the electrode adjacent to the solid electrolyte. Thus, on the first charge, a reaction front moves through the electrode towards the current collector in the centre; behind this reaction front, the electrode is fully charged and in front of it, fully discharged [6]. The first generation of ZEBRA cells (SL) utilised a cylindrical beta alumina tube and the positive electrode resistance increased significantly as the effective electrode thickness increased during discharge. This deficiency was overcome in the second generation ML cells by the use of a convoluted beta alumina tube (Fig. 5). This resulted in a 40% increase in the surface area of the beta alumina, thus reducing the contribution to the cell resistance by almost one-third [7]. It also results in a lower effective electrode resistance at any given depth of discharge. The overall effect is shown in Fig. 6. This reduction in cell resistance and consequent increase in maximum power capability, more than offset the extra weight of the electrolyte tube and the increased complexity of manufacture. When the charge is complete, no sodium chloride remains in the electrode. On the first discharge, the same process occurs, but the electrode is only partially discharged

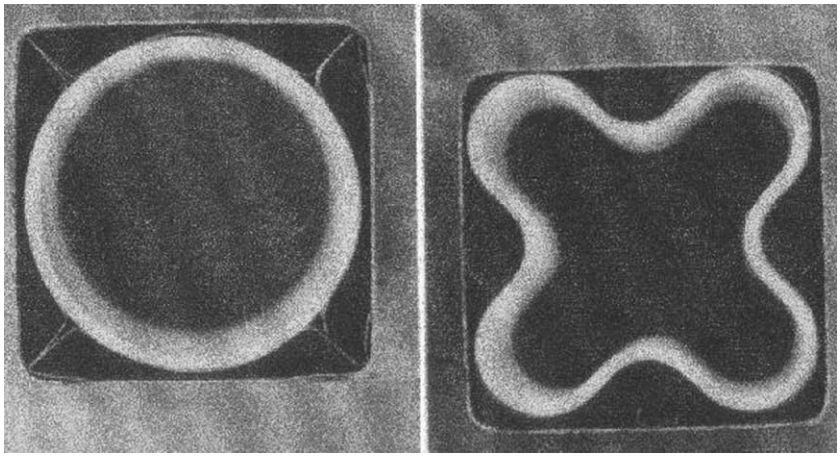

Fig. 5. Comparison of beta alumina tube cross-sections for SL/09 and ML/1G cells.

as the name plate capacity is less than the theoretical capacity. This results in a core of fully charged material remaining permanently in the centre of the electrode. The nickel chloride solubility is very low (see above) and this together with the presence of sulphur in the electrode, prevents recrystallisation and grain growth. If, however, the first charge is incomplete, sodium chloride crystals remain in the core of the electrode. These are much more soluble and grain growth is rapid. These large crystals disrupt the electrode structure and lead to loss of capacity.

A full charge on the first cycle is a necessary but not sufficient procedure to prevent capacity loss. Selection of the optimum charging procedure is essential. An IUI charging regime has been found to be the most effective and a typical charge curve is shown in Fig. 7. A current limit of 15 A per cell for a 32 Ah cell and a charging voltage of 2.67 V has been found to be optimum. Charge is terminated when current falls to 0.5 A per cell. Using this charging regime, stable capacity can be obtained over 3000 full cycles (Fig. 8). As can be seen from Fig. 9, the minimum time for a full charge is 5 h. Faster charging is possible by increasing the charge voltage to 2.85 V, but to prevent the cell resistance increasing, this should be restricted to 80% of the charge capacity. Fifty percent of the capacity can be recharged in 30 min and 80% in 75 min. For regenerative braking on electric vehicles, even faster charge rates are required and a charge voltage of up to 3.1 V is used. This is restricted to ca. 10% of the cell capacity but is available right up to top of charge.

Operation of cells in a battery presents few problems because of the characteristics of the ZEBRA cell. Thus, the 100% coulombic efficiency allows the state of charge to be

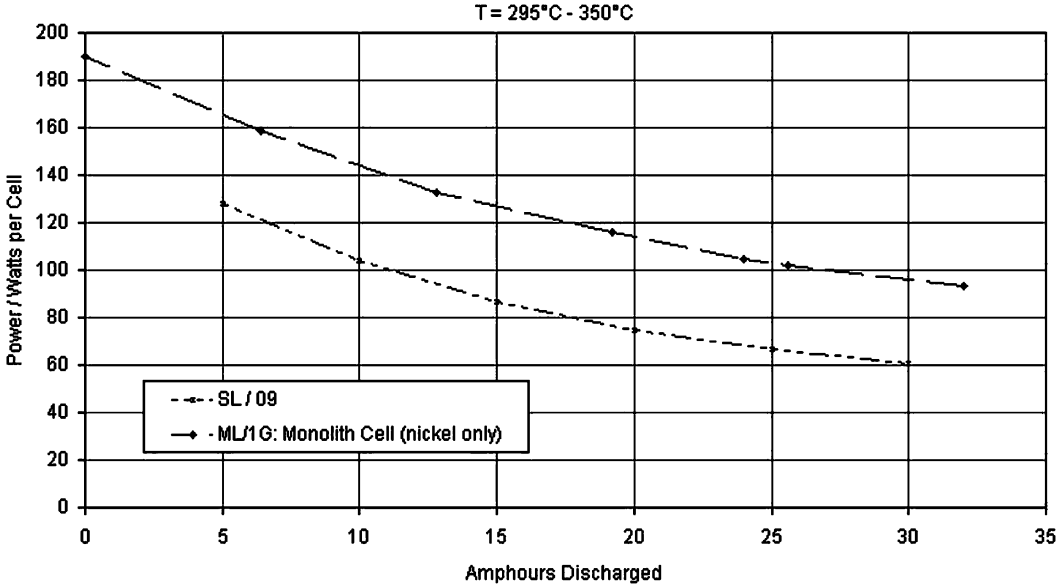

Fig. 6. Pulse power (30 s; 2/3 OCV) vs. %DoD.

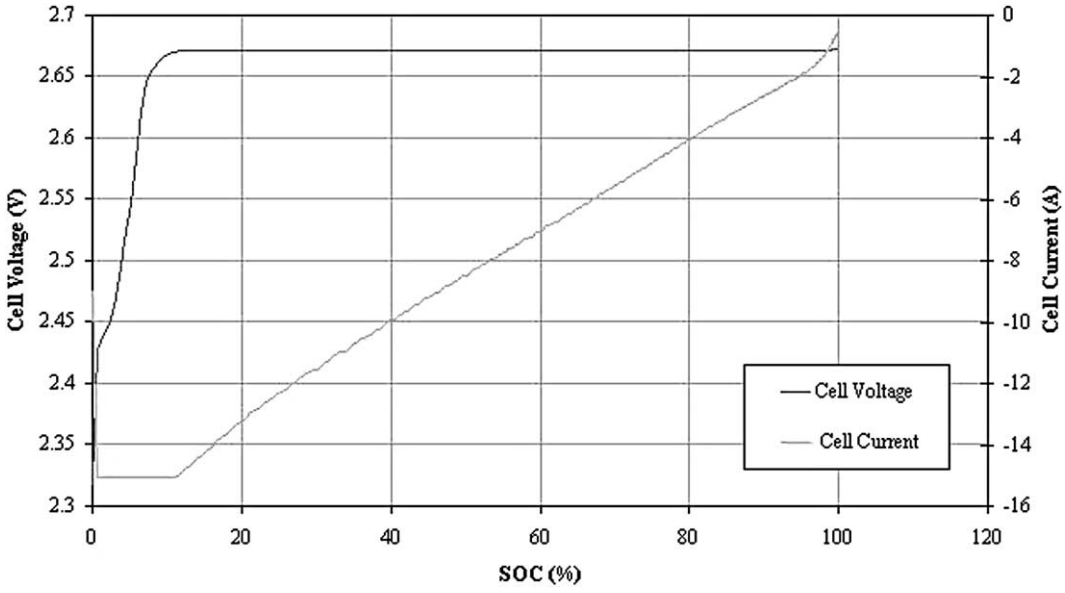

Fig. 7. Normal charge 100–0% DoD (2.67 V, 15–0.5 A).

monitored by measuring the ampere hours passed. The nameplate capacity of the cell is limited to ca. 75% of the theoretical capacity in order to meet the power specification at 80% DoD. This rather arbitrary end of discharge point is determined by coulometry. The electronic coulometers which are contained in the battery management interface (BMI) fitted to every battery, are re-set every time top of charge is reached, to maintain the accuracy of the coulometric measurements. The BMI also controls the battery temperature, by switching on heating or cooling as required, and controls the charging process. A number of algorithms have been developed for the BMI which keep the battery within the permitted operating window. The BMI communicates with the external load and battery charger via a CAN bus system and if any fault conditions develop, the battery is automatically isolated by two contactors located in the BMI.

Battery voltages up to 600 V can be achieved by series/parallel connections of the cells. An 18 kWh, 557 V battery would contain 216 cells connected in one series chain, whereas a 100 V battery of the same energy would have six parallel chains of 36 cells. This connection strategy is made possible by the failure mode of the cells. ZEBRA cells invariably fail to a resistance comparable to that of an intact cell. This means that a series chain can continue to operate with several cell failures, which makes the ZEBRA battery very robust. In a single chain battery, the only limit to the number of cell failures allowed is the reduction in energy

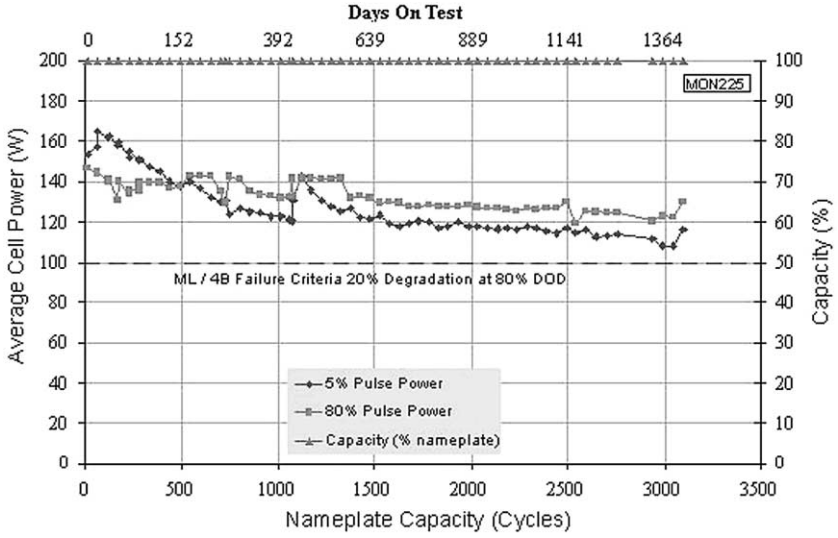

Fig. 8. Cycle life in 10-cell module on MB2a test.

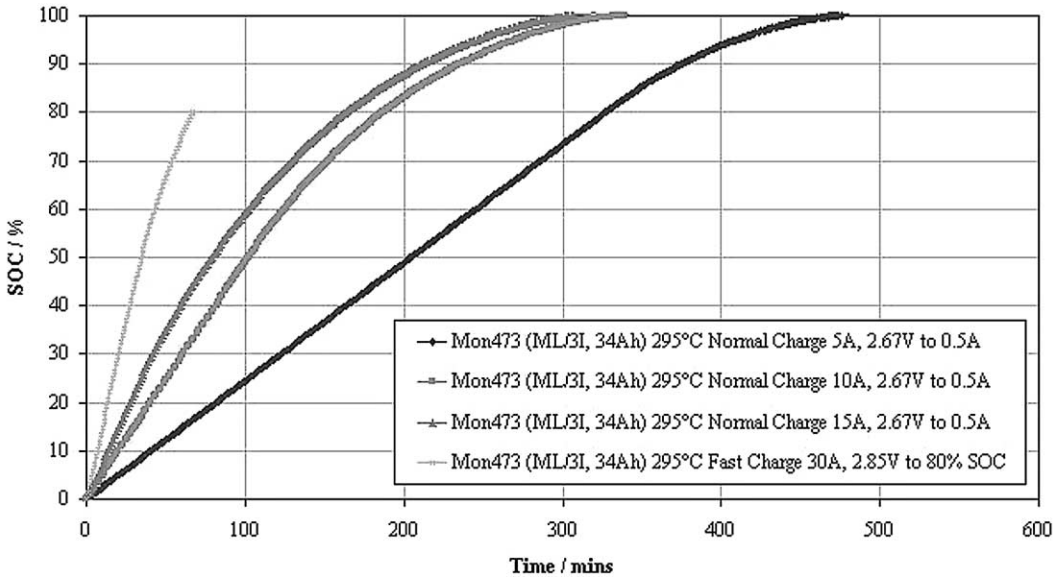

Fig. 9. Comparison of charge times for different charge regimes.

content which can be accepted. The BMI automatically adjusts the charging voltage to take account of the reduced open circuit voltage. For batteries with series/parallel connection, the number of permissible cell failures is determined by the extent to which chains of cells get out of balance — the higher the voltage, the more cell failures can be tolerated. For example, up to 5% cell failures can be tolerated in a 300 V battery. The main reason for this is that the charging voltage cannot be adjusted so accurately because the number of cell failures is more difficult to determine in a series/parallel connected battery. This characteristic of ZEBRA cells combined with the fitting of a BMI to the battery means that no cells ever have to be changed and it is a zero maintenance system.

Although the cells have 100% coulombic efficiency, and therefore, have no self discharge, the base operating temperature of 270°C requires that even in a very well insulated battery box utilising evacuated thermal insulation, some heat loss is inevitable. A 20 kWh battery would have a heat loss of around 80 W and this can be thought of as self discharge. It is not possible to quantify this as a percentage of capacity as it depends upon the operating cycle but it varies from 10% per day if the battery is not used at all to zero for an intensively used battery in which the temperature never falls to 270°C. It must be remembered, however, that this ''self discharge'' does not lead to cells getting out of balance and there are, therefore, no adverse effects other than a reduction in the energy available.

Although the high operating temperature can be a disadvantage in some applications, particularly those such as SLI batteries which are small in size and whose use is intermittent, for many applications the high operating temperature is a definite advantage. Thus, the characteristics of a ZEBRA battery are almost independent of ambient temperature. The electronic components in the BMI restrict the upper temperature limit to 70°C. There is effectively no lower temperature limit.

2. Cell life and performance characteristic

2.1. Specific power

As described above, the limitation to the specific power is the mode of operation of the positive electrode. When the reaction front is adjacent to the beta alumina, the resistance contribution from the positive electrode is very low. After even a short recharge, the reaction front moves back to the solid electrolyte and a deeply discharged cell will then exhibit the same resistance as a fully charged cell. This effect, of course, dissipates very quickly as the small amount of uncharged material is consumed and the reaction front reverts to its original position deep in the electrode.

This phenomenon suggested to Coetzer and Galloway an ingenious way of ensuring that high peak power pulses could be met, for a limited duration at least, at any state of charge [8]. By substituting a proportion of nickel in the electrode by iron, a second reaction becomes possible:

$$FeCl_2 + 2Na \rightarrow Fe + 2NaCl, \quad E = 2.35\,V \tag{7}$$

The original concept for the ZEBRA cell was as a sodium/iron II chloride cell and the chemistry of this cell is well established. It was superseded by the sodium/nickel chloride cell because of the latter's higher open circuit voltage, simpler chemistry ($FeCl_3$ which is formed on overcharge of iron cells is soluble in the sodium chloroaluminate melt) and wider temperature window.

In the presence of nickel, however, $FeCl_3$ cannot form as the emf of this cell is 2.76 V. In a mixed iron/nickel electrode, only the nickel takes part in the discharge reaction

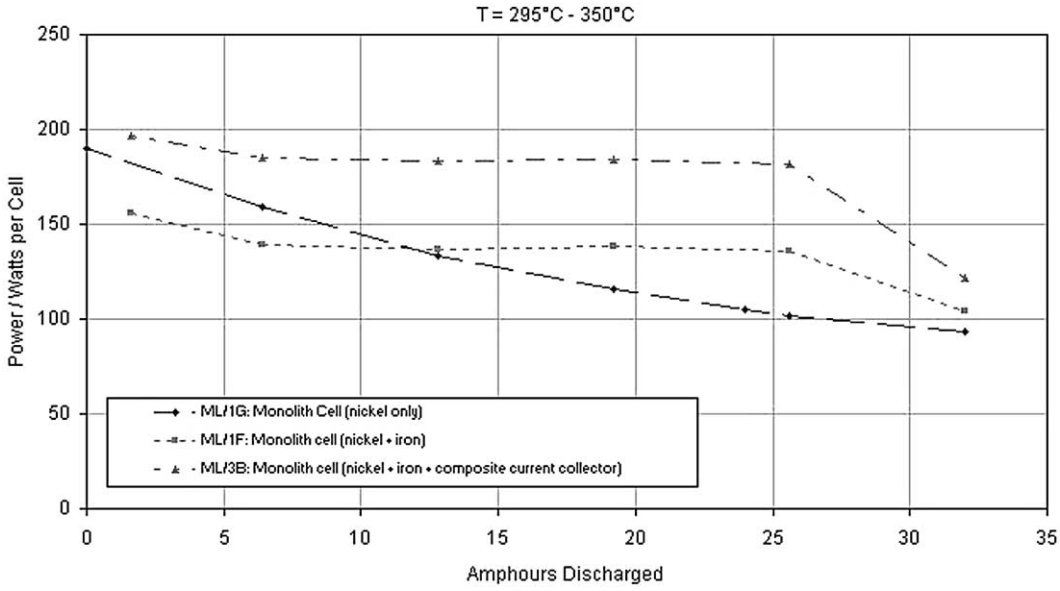

Fig. 10. Pulse power (30 s; 2/3 OCV) vs. % DoD.

at cell voltages above 2.35 V, iron being present as $FeCl_2$. When a load is applied which depresses the cell voltage below 2.35 V, the iron chloride can also discharge and for the reasons described above, this discharge starts adjacent to the beta alumina and thus, the positive electrode resistance is equivalent to that of a fully charged cell. As the iron is discharged, the reaction front moves through the electrode and the resistance increase, but for short pulses, the peak power is independent of depth of discharge. After the pulse, when the cell voltage rises above 2.35 V, iron chloride is reformed by the reaction

$$NiCl_2 + Fe \rightarrow Ni + FeCl_2 \quad (8)$$

This happens virtually instantaneously and the cell is immediately ready for another high power pulse. The values for the 30 s pulse power for the pure nickel system and the mixed nickel/iron system are shown as a function of depth of discharge in Fig. 10.

There is a small penalty in terms of specific energy as part of the cell capacity is discharged at a lower voltage but because the nickel capacity corresponds to 90% of the nameplate capacity (Fig. 11), the effect is very small (ca. 1%).

The incorporation of iron in the positive electrode has a second advantage: it prevents overdischarge of cells in batteries with several parallel chains. If cell failures occur

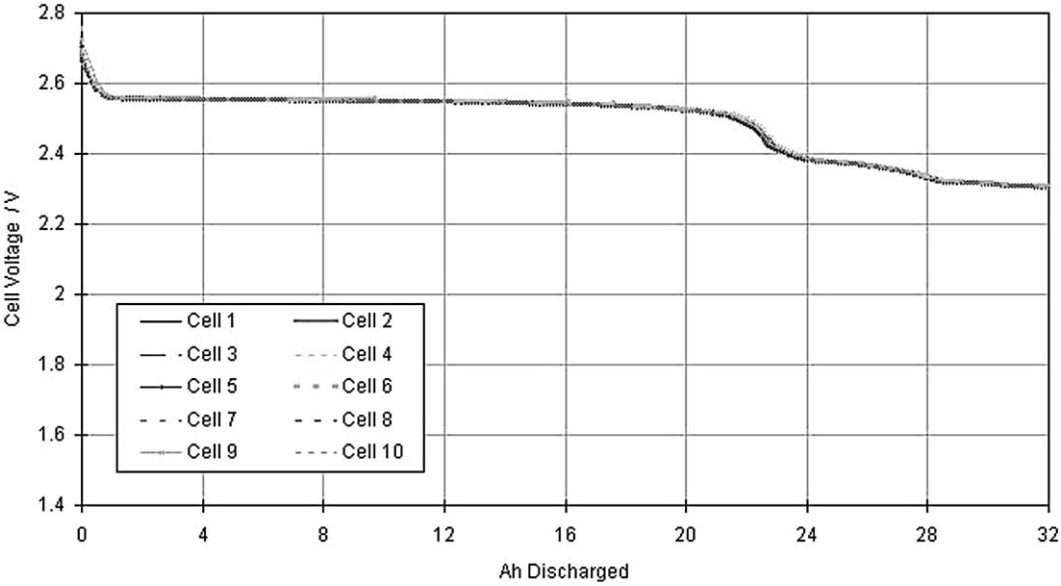

Fig. 11. ML/3I 32 Ah discharge at constant 1.5 A.

in one or more of the chains in a nickel battery, for any given load voltage, these chains will generate lower currents so that when the nameplate capacity is reached for the whole battery, these chains will be discharged less than the nominal capacity and the chains without failed cells will be discharged more. When the battery is switched off, internal circulating currents will continue to flow until (a) the chains with the failed cells are fully charged or (b) the cell in the chains without failures discharge onto a lower voltage plateau. In cells without iron, this plateau is reaction (6), which means that these chains become very deeply discharged with the risk of overdischarge if high currents are demanded. In batteries of iron-doped cells, this effect is much reduced as can be seen from Fig. 11 so that, for example in a two-hain 300 V battery, almost 10% of cells in one chain must fail before the chain can be fully charged by recirculating currents. This makes iron-doped batteries even more robust to cell failures than pure nickel batteries.

Not only does iron confer all the above advantages but substituting the much lower cost iron for around 20% of the nickel in the positive electrode, leads to a significant cost reduction.

A further reduction in cell resistance can be obtained by increasing the conductivity of the current collector. Nickel has a specific resistivity of $26 \times 10^{-6}\ \Omega$ cm at 300°C compared with copper at $3.7 \times 10^{-6}\ \Omega$ cm. Copper is electrochemically active and would corrode rapidly. Copper can be used, however, if it is clad with a nickel sheath [7]. Such composite wire made by drawing a composite billet is commercially available. This reduces the current collector resistance by 80%. Although the total cell resistance is reduced by less, this is still a worthwhile contribution to specific power improvement as can be seen from Fig. 10. This composite current collector is now made in-house by a different process which results in a lower cost than the pure nickel wire or the commercially available composite. The copper nickel ratio is 70:30 which results not only in a lower

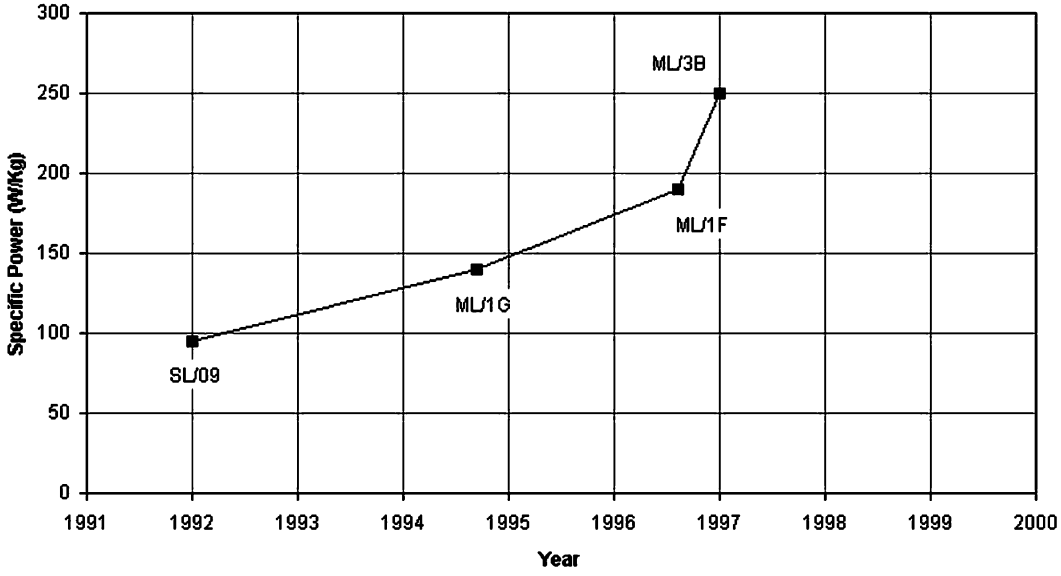

Fig. 12. Improvement in specific power of ZEBRA cells.

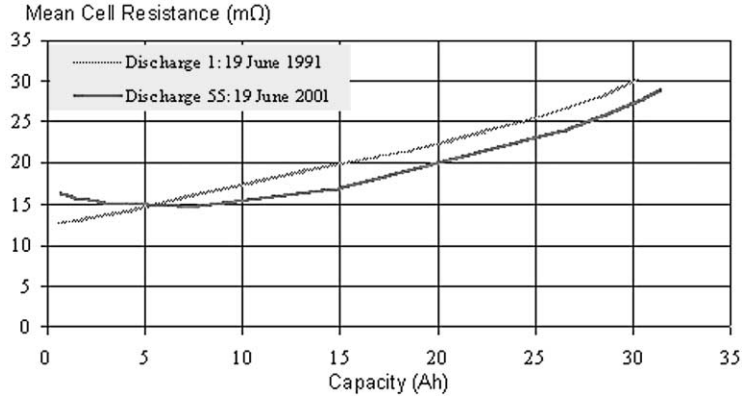

Fig. 13. Calendar life test.

resistance but a materials cost which is 20% of that of a pure nickel component.

The improvements in specific power of the ZEBRA cell, which the above development produced, are shown in Fig. 12.

2.2. Lifetime

The factors which determine cell life are: corrosion, resistance rise, and capacity loss. In the absence of electrical cycling, the ZEBRA cell degrades only very slowly as demonstrated by the performance of a small battery which was put on test in June 1991. This battery is held at top of charge on open circuit and over the last 10 years has had 55 charge/discharge cycles and eight freeze/thaw cycles. As can be seen from Fig. 13, the capacity is unchanged as is the cell resistance.

As that battery is still on test, it is not known how much, if any, corrosion has occurred or whether any changes have taken place in the electrodes. Such information, however, is available for a 10 cell battery module, which has been tested using a simulated electric vehicle regime (Figs. 14 and 15). This was taken off test after 4 years and over 3000 nameplate cycles. As can be seen from Fig. 16, it was still delivering its nameplate capacity. Although the internal resistance had risen, somewhat it was well below the end of life criteria of 20% degradation from the original specification. The pulse power at 80% was 96% of the initial specification.

One of the cells was dismantled and examined for indications of electrode degradation and corrosion. In the sodium electrode, the only sign of corrosion is to the glass seal This has a brown surface layer which extends only a few microns into the bulk of the glass. Underneath this layer, the glass is unaffected and the integrity of the glass seal has not been compromised at all.

The other seal in the cell is the thermocompression bond (TCB) seal between the alpha alumina collar to which the beta alumina tube is sealed and the two nickel components which are welded to the metal components in the two electrodes. This TCB seal is formed by applying a high load to the nickel components at around 1000°C for several minutes, whilst they are in contact with the alpha alumina collar [9]. A strong diffusion bond can be obtained when the metal components are bonded directly to the alpha alumina component, but because of the mismatch in expansion coefficients, the seal is susceptible to stress corrosion in the sodium chloroaluminate melt. This problem was overcome by metallising the alpha alumina with molybdenum. This reduces the stress in the bond to a level where stress corrosion is not a problem. The strengths of thermocompression bond seals in these cells were measured and found to be in the same range as new seals (2000–4000**N**) showing that no corrosion had occurred.

These cells contained an early version of the copper/nickel composite current collector. The composite wire was welded, not brazed, to the nickel filling tube through which the liquid electrolyte and positive electrode material are added to the cell. No significant corrosion of the current collector occurred except in the area of the weld where copper/nickel alloy was exposed to electrochemical action. In this region, a short length of the copper core had dissolved leaving the nickel sheath to carry the current. Despite this corrosion there was no noticeable effect on the cell

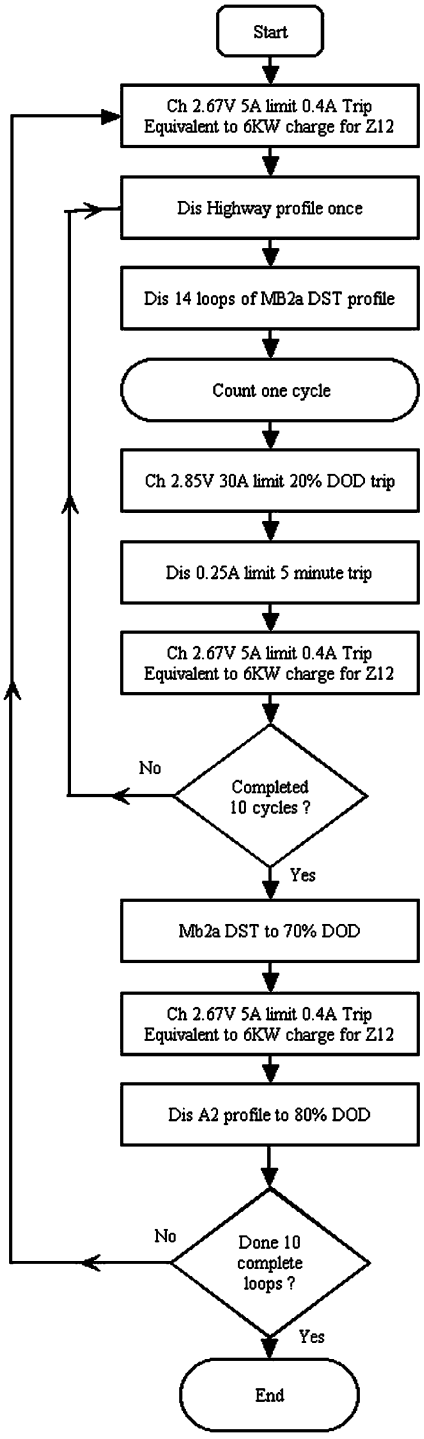

Fig. 14. MB2b car test.

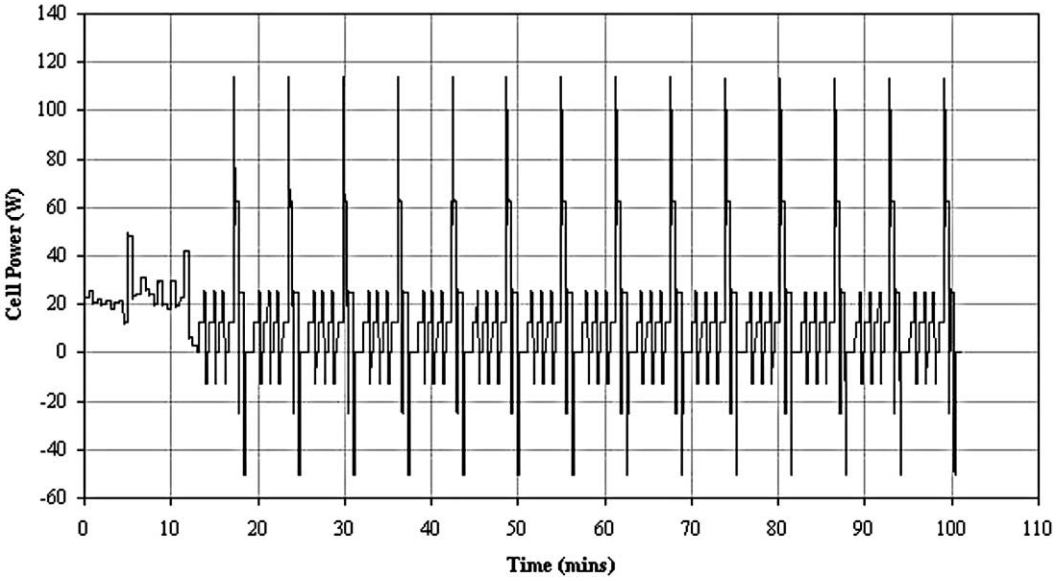

Fig. 15. Highway and DST discharge profile for MB2b test.

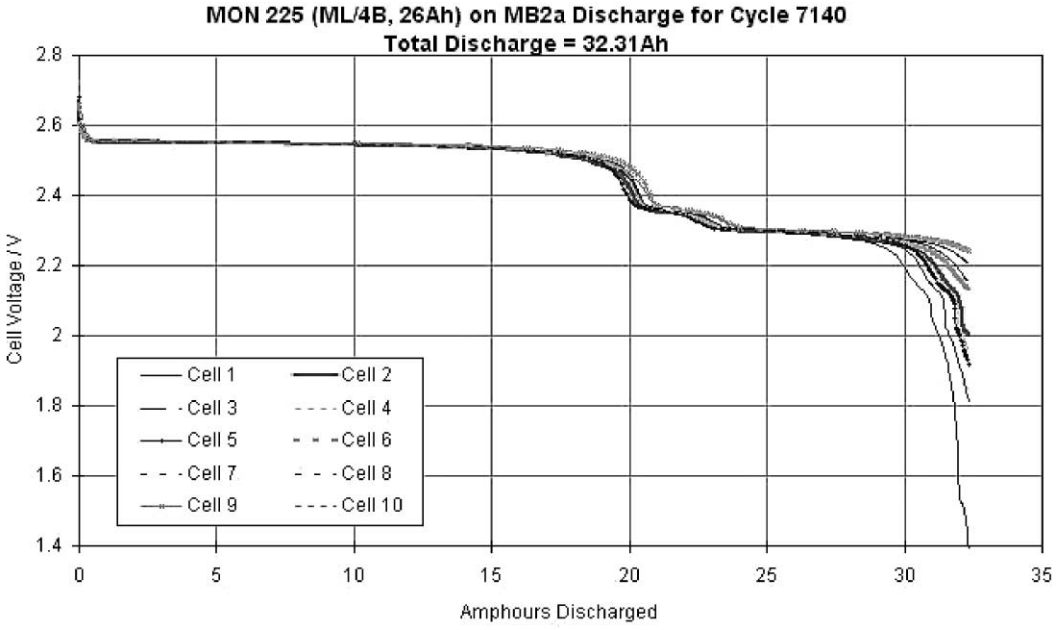

Fig. 16. The 10-cell module of ML/4B cells (nameplate capacity 26 Ah) on MB2a discharge for cycle 7140.

performance. As current cells have brazed joints, no corrosion should occur in this area.

3. Series production technology

Until recently, ZEBRA batteries have been produced in quantities of around 100 batteries per year on pilot line equipment in three centres in Germany and UK. At the beginning of 2001, a building for a new series production plant with a floor area of 18,000 m^2 was completed by the new owner of the ZEBRA technology, Carlo Bianco, at Stabio near Lugano in Switzerland (Fig. 17). This is the first phase of a factory which will eventually be capable of producing 100,000 batteries (each of around 20 kWh) per year. In this first phase, it is planned to produce 33,000 batteries per year, although enough space has been allowed for equipment to produce sufficient beta alumina powder for 100,000 batteries per year.

Fig. 17. New ZEBRA battery factory on the MES-DEA site in Stabio, Switzerland.

The production processes are based upon those developed on the pilot lines. The production of beta alumina powder is based upon the boehmite route [10]. The boehmite (aluminium oxide monohydrate $Al_2O_3 \cdot H_2O$) is calcined at around 800°C in an indirect gas fired rotary calciner at a rate equivalent to 4000 batteries per year. The calcined material which consists of a mixture of γ, δ, θ aluminas is mixed with sodium carbonate and lithium hydroxide in a pan granulator which produces a fine granulate suitable for the next process which is conversion to beta alumina. This is achieved using a direct gas fired rotary calciner at temperature of around 1200°C. The equipment presently in use can produce powder equivalent to 3000 batteries per year. The calcined powder is dispersed in water and milled to give a mean particle size between 1 and 2 μm using two flow-through bead mills. This produces a slurry containing around 60% solids which, after addition of organic materials to aid the isostatic pressing process, is spray dried to a powder with the necessary characteristics for automatic isostatic pressing. All this equipment is commercially available in sizes suitable for much larger quantities, and the plant will eventually have two lines each capable of producing powder equivalent to 50,000 batteries per year.

An automatic isostatic press with seven cavities has been installed and this will produce a compact every 20 s. Each compact has to be placed on a disc of compacted beta alumina powder, which in turn is placed on a fully dense spinel disc. Finally, a spinel tube is placed over the compact and locates on the spinel disc. The automatic handling equipment which assembles the individual parts places the assembly onto a mullite bat and transfers this bat to a kiln car. Six of these cars, each carrying 600 compacts are then loaded into a 9 m^3 capacity gas fired shuttle kiln. The firing profile is a continuous ramp up to 1570°C followed by a programmed cool down to 300°C, at which temperature the cars can be removed from the kiln. The whole firing cycle takes 24 h. The assembly is then automatically disassembled and the spinel components and mullite bats returned to their respective stores for re-use for up to 500 firings. From the shuttle kiln, the beta alumina tubes are conveyed by a monorail system to the cutting station where they are cut to length at the rate of three tubes per minute. From there, they are transported to a dye application station where a penetrative dye is applied to the inside and outside of the tube and then rinsed off with water and the tube dried. The tube is then inspected visually under UV light for defects which retain the dye. The good tubes are then measured using an automatic video measuring system and any tubes which fail the dimensional checks are rejected.

The equipment presently installed can produce tubes equivalent to 2000 batteries per year. The individual stations will be replicated as production demands increase with the exception of the shuttle kiln. Provision has been made for one further shuttle kiln which will be served by the same automatic handling equipment, but further increases in numbers will be achieved by the installation of a tunnel kiln.

The production of the thermocompression bond seal and its attachment to the beta alumina tube is achieved using three continuous walking beam furnaces. In the first furnace, the tubes are heated to around 1000°C in air to clean the surface. In a second furnace, the two nickel components are sealed to a metallised alpha alumina ring in a reducing atmosphere. When the parts have reached around 1000°C, a load of around 1 t is applied by the 15 rams of a multiple pressing head for a time long enough to allow interdiffusion at the nickel/molybdenum interface. Fifteen minutes is the minimum time and as each pressing mandrel accommodates four seals, the throughput can be as high as four seals per minute. The mean bond strength is ca. 2000 N which is more than adequate for the duty.

In the third furnace, the thermocompression bond seal is joined to the beta alumina tube by a fillet of glass. The glass is applied to a rebate in the alpha alumina collar in the form of a paste and the open end of the tube is placed over the rebate and onto the glass. Again the furnace operates at around 1000°C but in an atmosphere of nitrogen.

The ceramic sub-assembly is checked for helium leak tightness dimensional accuracy and the quality of the glass fillet joint before being passed on the cell assembly line. The steel bridging piece is welded to the outer nickel ring and the tube is coated with carbon powder using an aqueous suspension and dried in a batch oven. The assembly of the cell takes

place on a fully automated assembly line with a step time of 30 s. The steel shims which act as the sodium wick are wrapped around the tube and the assembly is pushed into the mild steel cell case. The sodium electrode compartment is sealed by laser welding the bridging piece to the cell case. The next step is to insert the current collector assembly, which includes the carbon felt blade, into the positive electrode compartment. The current collector is fabricated separately on an automatic machine from copper wire and nickel strip. The current collector is laser welded to the inner nickel ring and then the positive electrode granules are added. The granules are then vacuum dried in situ before the required volume of molten sodium chloroaluminate is dispensed into the cell. The final stage is to laser weld the positive cell top to the current collector.

In the pilot line, each cell was individually charged and discharged and various parameters measured. The operation took 24 h and on the series production line the procedure has been eliminated. Instead, the cells pass through an automatic X-ray examination which picks up any build faults.

The battery box is designed for low cost production. The cell pack is assembled separately using brazed copper intercell connectors. Between every other row of cells is a cooling plate through which air is circulated by an external blower. The cooling plates are fabricated from mild steel and they all connect into two plenum chambers, also fabricated from mild steel. This arrangement provides uniform cooling of all the cells in the battery pack when required. A composite resin/mica board containing heating elements sits on top of the cell pack and is used to heat up the battery initially and to maintain the base temperature of 270°C during use. Resin/mica sheets are sandwiched between cells for additional electrical insulation, allowing battery voltages up to 600 V to be specified. The cell pack is then inserted into the inner battery box.

The thermal insulation, a low density compressed powder board, fills the gap between the inner and outer battery boxes. The only metal connectors between the inner and outer battery boxes are the leadthrough for the positive and negative leads and the temperature monitoring leads, and the air inlet and outlet. Stainless steel bellows are used for low mechanical stress and low thermal conductivity.

When assembly is complete, the battery is placed in an oven at 300°C and the internal heaters switched on, heating the whole battery including the thermal insulation to around 300°C. During this period, the cavity between the inner and outer battery boxes is evacuated. This procedure desorbs moisture from the powder insulation and when this is complete, the vacuum connection is pinched off. Evacuating this cavity adds enormously to the strength of the battery box as the force resulting from atmospheric pressure creates a rigid monocoque structure. Once sealed, the vacuum is retained for the whole life of the battery.

Once the BMI has been connected, the battery is fully charged, discharged to check battery performance and the BMI function and then recharged and cooled down for despatch.

There are a number of battery types being produced using three cell types: ML/3 (32 Ah), ML/4 (26 Ah) and ML/8 (20 Ah). These correspond to three battery heights (300, 264 and 215 mm, respectively). The x and y dimensions can be changed according to the application. The battery which has been produced in the greatest numbers is the Z5 battery (Fig. 18) whose specification is given in Table 1. The plant capacities quoted above refer to Z5 batteries.

Fig. 18. ZEBRA battery.

Table 1
Z5 battery specification

	Battery type	
	Z5-278-ML-64	Z5-557-ML-32
Capacity (Ah)	64	32
Rated energy (kWh)	17.8	17.8
Open circuit voltage (V)	278.6	557
Maximum regen voltage (V)	335	670
Minimum operating voltage (V)	186	372
Maximum discharge current (A)	224	112
Cell type/no. of cells	ML3/216	ML3/216
Weight with BMI (kg)	195	195
Specific energy (Wh/kg)	91.2	91.2
specific power (W/kg)	164	164
Energy 2h discharge (Wh)	16	16
Peak power (kW)	32	32
Thermal loss (W)	<120	<120
Cooling	air	air
Heating time (h)	24 at 230 V ac	24 at 230 V ac
Ambient temperature (°C)	−40 to +70	−40 to +70
Dimensions, width (mm) × length (mm) × height (mm)	533 × 833 × 300	533 × 833 × 300

Table 2
Z11 and Z12 Battery specifications

	Battery type	
	Z11	Z12
Capacity (Ah)	96	104
Rated energy (kWh)	28.7	30
Open circuit voltage (V)	299.3	288.9
Maximum regen voltage (V)	359.6	347
Minimum operating voltage (V)	199.3	193
Maximum discharge current (A)	240	260
Cell type/no. of cells	ML3/348	ML4/448
Weight with BMI (kg)	335	375
Specific energy (Wh/kg)	85.6	80
Specific power (W/kg)	149	149
Energy 2h discharge (Wh)	25.8	26.5
Peak power (kW)	50	56
Thermal loss (W)	<160	<170
Cooling (kW)	2–6	2–8
Heating time (h)	24	24
Ambient temperature (°C)	−40 to +70	−40 to +70
Dimensions, width (mm) × length (mm) × height(mm)	903 × 676 × 315	992 × 794 × 278

4. Applications

4.1. Vehicles

The ZEBRA battery finds applications in both pure electric and hybrid vehicles. It is unique in being a completely self contained system complete with packaging, thermal management and a microprocessor controlled battery management system which provides an interface to the vehicle drive system. The battery pack itself is a no-maintenance unit as access to individual cells is not possible. The monocoque construction makes it extremely rugged as evidenced by the fact that it has passed all the safety tests devised by European car manufacturers (EUCAR) [11]. For electric cars, several battery types have been developed. Two 30 kWh batteries were developed — the Z12 based on ML/4 cells and the Z11 based on ML/3 cells.

The Z12 was liquid cooled and had an oil/water heat exchange which interfaced with the vehicle heating system. It was installed in the Mercedes A class and a small fleet of these vehicles built in 1998 is still operating [12]. With a range of over 100 miles, and good acceleration, gradeabilty and climate control, the electric A class was almost indistinguishable from the internal combustion engine version.

The Z11 battery was also liquid cooled and was installed in BMW 3 series cars [13]. The specific energy of the Z11 was slightly higher than that of the Z12 battery (Table 2) but the performance of the car was very similar.

The 17 kWh Z5 battery has been used in several cars including the Renault Twingo and Clio, the Opel Astra, the Mercedes Benz 190 and the BMW 3 series [14]. The Z5 is also the preferred battery for larger vehicles such as delivery vans and buses. ZEBRA batteries are possibly unique in that individual batteries can be connected in parallel using a multi-battery server (MBS). The MBS can operate up to 10 individual batteries via the BMI on each battery. The main function of the MBS is to provide a single interface to the drive system. It can also reduce the overall charge voltage should any cell failures occur. The preferred strategy for normal rate charging is to have one charger per battery. This gives a completely modular system and also maintains the full charging voltage on all the batteries which have no cell failures.

Several pure electric battery buses with up to six Z5 batteries are in service in the Italian cities of Bologna, Florence and Modena giving totally emission free operation.

Table 3
B5 battery specification[a]

	B5-26-ML-39 battery
Capacity (Ah)	310
Rated energy (kWh)	8
Open circuit voltage (V)	25.8
Maximum regen voltage (V)	–
Minimum operating voltage (V)	17.2
Maximum discharge current (A)	112
Cell type /no. of cells	ML3/80
Weight with BMI (kg)	78
Specific energy (Wh/kg)	103
Specific power (W/kg)	151
Energy 2 h discharge (Wh)	7.2
Peak power (kW)	11.8
Thermal loss (W)	<55
Cooling	none
Heating time (h)	24 at 230 V ac
Ambient temperature (°C)	−40 to +70
Dimensions without BMI (length × width × heigth) (mm × mm × mm)	455 × 350 × 305

[a] The specific energies quoted are nominal figures, i.e. OCVx Ah/total weight.

In addition, there are a number of diesel/battery hybrid buses in service. These have a 1.9 l diesel engine which runs at constant power and two or three Z5 batteries. The vehicles can operate in two modes: full battery operation for sensitive areas of the city, hybrid mode when the battery either supports the diesel engine or is charged by the diesel engine. In both cases, regenerative braking is available. Z5 batteries have also been installed in Mercedes Benz Vito and Sprinter delivery vans.

4.2. Telecommunications

This is in many ways an ideal application for ZEBRA batteries. The battery is permanently connected to the power supply and is floated close to the open circuit voltage in the fully charged state. Discharge will only occur when the power supply fails. These conditions are very similar to those of the calendar life test described above which showed no deterioration in performance after 10 years.

The specification of a telecommunication battery is shown in Table 3. The specific energy is higher than that of electric vehicle batteries as there is no requirement for a high power pulse. This allows the nameplate capacity of the cell to be increased from 32 to 40 Ah. The optimum float voltage for a ZEBRA cell is 2.60 V. A simplified battery management system is incorporated into the power supply. This will control the battery temperature at 270°C and the float voltage at 2.60 V per cell. It also monitors the battery current and state of charge. Any faults in the battery will produce current perturbations which means that the health of the battery can be continuously monitored.

This is a new application for ZEBRA battery and a joint development programme is in progress with a Telecom company to produce prototype batteries for field trials. The wide operating temperature range of the ZEBRA battery makes it suitable for installation in many locations whose climate would otherwise preclude the use of standby batteries.

4.3. Marine applications

Electric propulsion is well established in one marine application — submarines — but there is an increasing interest in the use of batteries in other marine applications [15]. The concept of the ''Electric Ship'' is gaining ground. The primary power source is a gas turbine but a battery storing up to 1 MWh is provided to maintain power during, for example, switchover from one turbine to a second turbine which requires up to 1 MW for the duration of the changeover. In both surface ships and in submarines, the compactness and lightweight of ZEBRA batteries are an advantage but the long life, high integrity and zero maintenance characteristics are probably more valuable.

In conventional submarine applications, there is a choice of a 55% weight saving (for similar energy storage) or a combination of extra energy storage and a weight saving (compared with lead acid batteries). Because of the operational requirements of a submarine, a nominal 35% extra capacity could nearly double the energy available for planned use in low speed patrolling or during snorting transit.

In a nuclear submarine, the advantages are the safety value of the increased reserves and the elimination of routine battery maintenance.

5. Current status and future prospects

Since 1999, when MES purchased the ZEBRA battery technology, considerable progress has been made in the commercialisation of the ZEBRA battery. Cost reduction has been the principal objective during this period and the experience of MES in the highly automated production of automotive components has been brought to bear on the ZEBRA battery. This has resulted in substantial reductions in the cost of cell components particularly the cell case which is now fabricated from sheet rather than an eight stage deep drawing process, and the current collector which is fabricated on a continuous line instead of using a wire drawing process with several annealing steps followed by a batch brazing process to join the wire to the filling tube.

The battery housing together with the internal cooling panels have been redesigned for series production with associated cost reductions. The cells are now assembled into the battery straight from the production line with no electrical testing until the first charge of the battery.

The processing of the ceramic electrolyte has been highly automated and is now at the same level of automation as the cell production. This has been achieved by the construction of a purpose built factory and the installation of the existing pilot line equipment together with new production equipment, to give an initial production rate of 2000 batteries per year. It is planned to increase this capacity in stages to 33,000 batteries per year and space is available on the site for further expansion to a maximum of 100,000 batteries per year.

A wide range of battery types can be produced to suit specific applications. All batteries are fully sealed and completely self contained with heating and cooling system and battery management interface.

The key to achieving long calendar life and cycle life is the battery management interface. Algorithms have been developed to control the key parameters which affect life, i.e. charge regime including normal charging, fast charging and regenerative braking; end of discharge and operating temperature. As these algorithms are developed and improved, the life of the battery in the field will approach its ultimate value as demonstrated in controlled laboratory tests.

Bench testing has shown that the calendar life is at least 10 years and may be as long as 20 years, and the cycle life in an electric car applications should be in excess of 3000 nameplate cycles.

References

[1] J. Coetzer, in: Proceedings of the 170th Meet of Electrochemical Society, San Diego, CA, USA, October 1986, Extended Abstract No. 762.

[2] R.C. Galloway, J. Electrochem. Soc. 134 (1987) 1.

[3] R.J. Wedlake, J. Coetzer, I.L. Vlok, Power Sources 12, International Power Sources Committee, Leatherhead, UK, 1988, p. 563.

[4] R.J. Bones, D.A. Teagle, S.D. Brooker, F.L. Cullen, in: Proceedings of the Fall Meeting of Electrochemistry Society, Honolulu, HI, USA, October 1987, Extended Abstract No. 158.

[5] M.G. MacMillan, B. Cleaver, J. Chem. Soc. Faraday Trans. 89 (1993).

[6] N.D. Nicholson, D.S. Demott, R. Hutchings, Proc. Intl. Power Sources Symp., 1988, paper no. 37.

[7] J. Coetzer, J.L. Sudworth, A Second Generation Sodium Nickel Chloride ZEBRA Cell, EVS 13, Osaka, October 1996.

[8] R.C. Galloway, S. Haslam, J. Power Sources 80 (1999) 164–170.

[9] D.J. Baker, W.G. Bugden, P.R. Smith, US Patent 5,009,357, 1991.

[10] J.H. Duncan, P. Barrow, P.Y. Brown, in: Proceedings of British Ceramics on Electroceramics, Vol. 41, 1989.

[11] H. Boehm, R.N. Bull, A. Prassek, ZEBRA's Response to the New EVCAR/USABC Abuse Test Procedure, EVS15, Brussels, 1998.

[12] J. Gaub, A. Van Zyl, Mercedes Benz Electric Vehicles with ZEBRA Batteries, EVS 14, Orlando, December 1997.

[13] H.H. Kranz, F. Better, R. Hoeppler, A. Prassek, ZEBRA Z11 in BMW Test Carriers, EVS 14, Orlando, December 1997.

[14] R. Bady, J.W. Biermann, B. Kaufmann, H. Hacker, European Fleet Demonstration with ZEBRA Advanced Batteries, 1999 SAE International Congress and Exposition, Detroit, 1999.

[15] A.J. Donaldson, AIP and Advanced Batteries: Technologies to Change Tomorrow's Navies. Naval Technology Seminar, Singapore, May 2001.